

Curve Tracking Control for Autonomous Vehicles with Rigidly Mounted Range Sensors

Jonghoek Kim · Fumin Zhang · Magnus Egerstedt

Received: 15 April 2008 / Accepted: 12 January 2009 / Published online: 11 February 2009
© Springer Science + Business Media B.V. 2009

Abstract In this paper, we present feedback control laws for an autonomous vehicle with rigidly mounted range sensors to track a desired curve. In particular, we consider a vehicle that has a group of rays around two center rays that are perpendicular to the velocity of the vehicle. Under such a sensor configuration, singularities are bound to occur in the curve tracking feedback control law when tracking concave curves. To overcome this singularity, we derive a hybrid strategy of switching between control laws when the vehicle gets close to singularities. Rigorous proof and extensive simulation results verify the validity of the proposed feedback control law.

Keywords Autonomous vehicle · Curve tracking · Switching systems

1 Introduction

Curve tracking control is fundamental for autonomous vehicles following desired paths, e.g., staying in lanes or avoiding obstacles. An example in which this becomes relevant is when an autonomous vehicle is to follow the curb or the lane markings. Figure 1 shows the autonomous vehicle Sting-I that represented Georgia Tech in the DARPA Urban Grand Challenge in 2007. As one of this vehicle's lane perception strategies, two rigidly mounted range sensors (lidars) were installed on both sides of the vehicle. At each instant of time, the vehicle emits a group of laser rays around the center ray forming a fixed angle with the velocity of the vehicle. When the center

J. Kim · F. Zhang (✉) · M. Egerstedt
Electrical and Computer Engineering, Georgia Institute of Technology, Atlanta, GA, USA
e-mail: fumin@ece.gatech.edu

J. Kim
e-mail: jkim37@mail.gatech.edu

M. Egerstedt
e-mail: magnus@ece.gatech.edu

Fig. 1 The Sting-1 vehicle at Georgia Tech



ray intersects a lane, it detects a point on the lane. From the distance measurements taken by the rays around the center ray, the autonomous vehicle is able to estimate the curvature of the lane at the point, the distance from the point, and the angle between the heading vector of the vehicle and the tangent vector to the lane.

In this paper, we design a curve tracking control law that uses these measurements as feedback to create the desired lane-following behavior to be used as a component in the Georgia Tech urban grand challenge system. It should be noted that our results can be applied to other types of autonomous vehicles with similar range sensor configurations.

The literature is abundant with papers on curve tracking for autonomous vehicles. For example, in [1], a reference point moves along the reference trajectory while the vehicle follows it, and the reference point might stop to wait for the vehicle. In [2] and [3], a gyroscopic feedback law was used to control the model that describes the interaction between the vehicle with an image particle representing the closest point on a closed curve bounding an obstacle. This controller design method was extended to set up cooperative motion patterns on closed curves for multiple vehicles in [4–6] and generalized to the design of tracking laws in three dimensions in [7] and [8]. The closest point is also used for path following in [9]. In [10], vehicles collect measurements at multiple fixed points in front of the vehicle and a recursive spline is updated and followed by feedback control. Similarly, the problem of tracking a ground curve is formulated as controlling the shape of the curve in the image plane in [11]. A biologically plausible feedback law that achieves motion camouflage that is related to curve tracking is shown in [12]. The authors of [13] determined bounds for the sampling intervals so that the vehicle stays in the lane with limited sensing rate. A feedback linearization approach and Lyapunov-oriented control designs were presented to make a mobile vehicle converge to a predefined path in [14]. Curve tracking for an atomic force microscope was considered in [15]. The authors of [16] presented a decentralized coordination algorithm for multiple vehicles to locate and track a dynamic perimeter. In addition, vision-based path following methods could be found in [17–21]. Various other path planning methods were introduced in [22–28].

In the literature reviewed above, curve tracking control usually have difficulties when the curve is concave, i.e., curving towards the vehicle. In this paper, we follow

a similar procedure as in [2] to develop the curve tracking control laws for both convex and concave curves based on Lyapunov functions. However, our results are significantly different and, hence, complementary to those in [2]. First, information of the closest point is used in [2], which requires wide-aperture scanning sensors. The methods in this paper only require two narrow-aperture range sensors pointing to a fixed direction relative to the moving direction of the vehicle to gather information at the detected points. Using detected points not only makes the tracking dynamics more complicated, but it also causes singularities in control laws when tracking concave curves. We show that these singularities cannot be avoided by changing the shape of the Lyapunov function used in [2]. Therefore, to overcome singularities of the Lyapunov function-based control laws, we develop switching controllers to make the system asymptotically stable. The switching strategy that achieves curve tracking with narrow-aperture-range sensors is our main contribution in this paper, which has not been achieved in the references.

The proof of the convergence of our switching control laws is inspired by convergence results for switching systems in the literature. Conditions for nonlinear switching systems to be asymptotically stable were presented in [29]. In [30–32], multiple Lyapunov functions were used to prove stability. In [33], the authors proposed control laws that switch between an approximate control when the system is near a singularity and an exact control when the system is bounded away from the singularity.

This paper is organized as follows: In Section 2, we present a system model for curve tracking with rigidly mounted sensors. In Section 3, we select a Lyapunov function for the convergence analysis and derive a feedback control law to asymptotically stabilize this system. Furthermore, to avoid the singularity where the denominator of the feedback control law is zero, switching control laws are developed with provable convergence. In Section 4, simulation results are presented. A summary and directions for future research are discussed in Section 5.

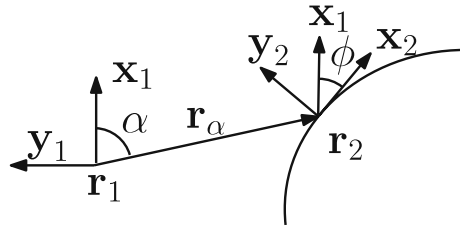
2 Boundary-Following Model with Rigidly Mounted Range Sensors

Consider a vehicle with two range sensors that emit center rays forming a fixed angle α with the velocity of the vehicle. When a boundary curve is presented in the plane, the center ray will intersect the boundary and detect a point \vec{r}_2 , which will be called the *detected point*. Here, \vec{r}_1 is the position of the vehicle. Hence, the relative position between the vehicle and the detected point is $\vec{r}_\alpha = \vec{r}_2 - \vec{r}_1$, and ϕ is the angle measured counterclockwise from the tangent vector \vec{x}_2 at the detected point to the heading direction of the vehicle \vec{x}_1 .

We first establish two Frenet–Serret frames [18]: one at the vehicle, the other at the detected point, as shown in Fig. 2. These two frames satisfy the Frenet–Serret equations:

$$\begin{aligned}
 \dot{\vec{r}}_1 &= v_1 \vec{x}_1 \\
 \dot{\vec{x}}_1 &= v_1 u \vec{y}_1 \\
 \dot{\vec{y}}_1 &= -v_1 u \vec{x}_1
 \end{aligned} \tag{1}$$

Fig. 2 A vehicle with a rigidly mounted sensor at angle α and a boundary curve in its environment



$$\begin{aligned} \dot{r}_2 &= \dot{s}\vec{x}_2 \\ \dot{x}_2 &= \dot{s}\kappa\vec{y}_2 \\ \dot{y}_2 &= -\dot{s}\kappa\vec{x}_2, \end{aligned} \tag{2}$$

where v_1 is the speed control and u is the steering (i.e., curvature) control we apply to avoid colliding with the obstacle and to achieve boundary following. In addition, κ is the curvature of the curve at the detected point obtained using a group of rays around the center ray, and s is the arc-length parameter of the curve. We may choose the positive direction of the boundary curve such that

$$\vec{x}_1 \cdot \vec{x}_2 = \cos(\phi) > 0. \tag{3}$$

When the curve is convex, i.e., curving away from the vehicle, we have $\kappa < 0$. When the curve is concave, i.e., curving towards the vehicle, the curvature $\kappa > 0$. The above settings for the interaction between the vehicle and the boundary curve were introduced in [2].

The key idea of curve tracking control is to control the relative motion between the vehicle and the detected point. For this purpose, we develop a set of equations that govern the relative motion.

The relative position between the vehicle and the detected point is ($\vec{r}_\alpha = \vec{r}_2 - \vec{r}_1$). In Fig. 2, α is defined as the angle formed by \vec{r}_α and \vec{x}_1 . Also, let $r_\alpha = \|\vec{r}_\alpha\|$. Then,

$$\vec{r}_\alpha \cdot \vec{x}_1 = \cos(\alpha)r_\alpha. \tag{4}$$

To derive the relative motion equations, we need to find \dot{r}_α , \dot{s} , and $\dot{\phi}$.

We first obtain an equation linking \dot{r}_α with \dot{s} . Take the time derivative of \vec{r}_α using Eqs. 1 and 2 to get

$$\dot{\vec{r}}_\alpha = \dot{s}\vec{x}_2 - v_1\vec{x}_1. \tag{5}$$

Differentiating Eq. 4 with respect to time on both sides, we obtain

$$\dot{\vec{r}}_\alpha \cdot \vec{x}_1 + \vec{r}_\alpha \cdot \dot{\vec{x}}_1 = \cos(\alpha)\dot{r}_\alpha. \tag{6}$$

Then, replacing $\dot{\vec{x}}_1$ by $v_1u\vec{y}_1$, we get

$$\dot{\vec{r}}_\alpha \cdot \vec{x}_1 + \vec{r}_\alpha \cdot v_1u\vec{y}_1 = \cos(\alpha)\dot{r}_\alpha. \tag{7}$$

Replacing $\dot{\vec{r}}_\alpha$ in Eq. 7 by Eq. 5, we obtain

$$(\dot{s}\vec{x}_2 - v_1\vec{x}_1) \cdot \vec{x}_1 + \vec{r}_\alpha \cdot v_1u\vec{y}_1 = \cos(\alpha)\dot{r}_\alpha. \tag{8}$$

We observe that, in Fig. 2, the angle formed by \vec{x}_1 and \vec{x}_2 is ϕ , and the angle formed by \vec{r}_α and \vec{y}_1 is $(\frac{\pi}{2} + \alpha)$. Therefore, since $\vec{x}_1 \cdot \vec{x}_2 = \cos \phi$ and $\vec{r}_\alpha \cdot \vec{y}_1 = -\sin \alpha$, we get from Eq. 8

$$\dot{s} \cos(\phi) = v_1(1 + \sin(\alpha)r_\alpha u) + \cos(\alpha)\dot{r}_\alpha. \tag{9}$$

Now, noticing that

$$r_\alpha^2 = \|\vec{r}_\alpha\|^2 = \vec{r}_\alpha \cdot (\vec{r}_2 - \vec{r}_1), \tag{10}$$

an equation linking \dot{r}_α with \dot{s} can be established. We differentiate Eq. 10 with respect to time on both sides to obtain

$$2r_\alpha\dot{r}_\alpha = 2(\dot{s}\vec{r}_\alpha \cdot \vec{x}_2 - v_1\vec{r}_\alpha \cdot \vec{x}_1), \tag{11}$$

where we have used Eq. 5. Then, \dot{r}_α is

$$\dot{r}_\alpha = \dot{s} \frac{\vec{r}_\alpha}{r_\alpha} \cdot \vec{x}_2 - v_1 \cos(\alpha), \tag{12}$$

where we used the fact that, in Fig. 2, the angle formed by \vec{r}_α and \vec{x}_1 is α . We also observe that the angle formed by \vec{r}_α and \vec{x}_2 is $(\alpha - \phi)$. Hence,

$$\frac{\vec{r}_\alpha}{r_\alpha} \cdot \vec{x}_2 = \cos(\alpha - \phi). \tag{13}$$

Replacing the term $\frac{\vec{r}_\alpha}{r_\alpha} \cdot \vec{x}_2$ in Eq. 12 by Eq. 13 gives

$$\dot{r}_\alpha = \dot{s} \cos(\alpha - \phi) - v_1 \cos(\alpha). \tag{14}$$

We can now find \dot{r}_α and \dot{s} . Substituting the term \dot{r}_α in Eq. 9 for Eq. 14, we obtain

$$\begin{aligned} \dot{s} \cos(\phi) &= v_1(1 + \sin(\alpha)r_\alpha u) \\ &+ \cos(\alpha)(\dot{s} \cos(\alpha - \phi) - v_1 \cos(\alpha)). \end{aligned} \tag{15}$$

Therefore, we obtain the time derivative of arc-length \dot{s} as

$$\dot{s} = \frac{v_1(r_\alpha u + \sin(\alpha))}{\sin(\alpha - \phi)}. \tag{16}$$

The term \dot{s} in Eq. 14 can be replaced by \dot{s} in Eq. 16 to get \dot{r}_α as follows:

$$\dot{r}_\alpha = v_1 \frac{\sin(\phi) + r_\alpha u \cos(\alpha - \phi)}{\sin(\alpha - \phi)}. \tag{17}$$

Now, let us find the equation for $\dot{\phi}$. From Fig. 2, we can see that the angle between \vec{x}_1 and \vec{y}_2 is $(\frac{\pi}{2} - \phi)$; hence,

$$\sin(\phi) = \vec{x}_1 \cdot \vec{y}_2. \tag{18}$$

Also, in Fig. 2, the angle formed by \vec{r}_α and \vec{y}_2 is $(\frac{\pi}{2} + \alpha - \phi)$ so that

$$\vec{r}_\alpha \cdot \vec{y}_2 = -r_\alpha \sin(\alpha - \phi). \tag{19}$$

Differentiating Eq. 13 with respect to time on both sides obtains

$$\sin(\alpha - \phi) \cdot \dot{\phi} = \frac{\dot{s} - v_1 \cos(\phi)}{r_\alpha} - \frac{\dot{s} \cos(\alpha - \phi) - v_1 \cos(\alpha)}{r_\alpha} \cdot \cos(\alpha - \phi) - \dot{s} \kappa \sin(\alpha - \phi), \tag{20}$$

where we have used Eqs. 2, 5, 13, 14, and 19. Therefore, the equation for $\dot{\phi}$ is

$$\dot{\phi} = v_1 \left(-\frac{\kappa \sin(\alpha)}{\sin(\alpha - \phi)} + u \left(1 - \frac{r_\alpha \kappa}{\sin(\alpha - \phi)} \right) \right), \tag{21}$$

where Eq. 16 is also used.

For the Sting-I autonomous vehicle, the sensor on each side of the vehicle is installed such that $\alpha = \frac{\pi}{2}$. In this case, Eq. 16 is simplified to

$$\dot{s} = \frac{v_1(r_\alpha u + 1)}{\cos(\phi)}, \tag{22}$$

Eq. 17 is simplified to

$$\dot{r}_\alpha = v_1 \tan(\phi)(1 + r_\alpha u), \tag{23}$$

and Eq. 21 is simplified to

$$\dot{\phi} = v_1 \left(-\frac{\kappa}{\cos(\phi)} + u \left(1 - \frac{r_\alpha \kappa}{\cos(\phi)} \right) \right). \tag{24}$$

The system equations are significantly different from the equations for the closest point in [2].

3 Controller Design and Convergence Analysis

3.1 Lyapunov Function

Consider the Lyapunov function candidate:

$$V_1 = -\ln(\cos(\phi)) + h(r_\alpha), \tag{25}$$

where $h(r_\alpha)$ satisfies the following conditions:

1. $dh/dr_\alpha = f(r_\alpha)$, where $f(r_\alpha)$ is a Lipschitz continuous function on $(0, \infty)$, so that $h(r_\alpha)$ is continuously differentiable on $(0, \infty)$.
2. $\lim_{r_\alpha \rightarrow 0} f(r_\alpha) = -\infty$, which leads to $\lim_{r_\alpha \rightarrow 0} h(r_\alpha) = \infty$. This is needed to blow up V_1 as the moving vehicle approaches collision with the boundary curve.
3. $f(r_\alpha)$ vanishes at a point where $r_\alpha = r_0$ and $h(r_\alpha)$ assume a local minimum in order for the moving vehicle to converge to the desired relative position at a distance from the boundary curve given by $r_\alpha = r_0$.
4. $\lim_{r_\alpha \rightarrow \infty} h(r_\alpha) = \infty$. This condition and the form of V_1 suggest that V_1 is radially unbounded (i.e., $V_1 \rightarrow \infty$ as $\|\phi\| \rightarrow \pi/2$, as $r_\alpha \rightarrow 0$, or as $r_\alpha \rightarrow \infty$).

Observe that V_1 , given by Eq. 25, is continuously differentiable because of Eq. 3. The term $\ln(\cos(\phi))$ penalizes misalignment between the velocity vector of the moving vehicle with the tangent vector to the boundary curve at the detected point. The term $h(r_\alpha)$ in Eq. 25 deals with the separation between the moving vehicle and the boundary curve. In short, V_1 is designed to make a vehicle converge to the relative position where $r_\alpha = r_0$ and $\phi = 0$. This form of Lyapunov function has also been used in curve tracking using the closest point information in [2] and [6].

For the point detected by the fixed center ray at an angle $\alpha = \pi/2$, our candidate $f(r_\alpha)$ satisfying these conditions is

$$f(r_\alpha) = \frac{-1}{r_\alpha} + \frac{1}{r_0}. \tag{26}$$

Further, the corresponding $h(r_\alpha)$ is

$$h(r_\alpha) = -\ln(r_\alpha) + \frac{r_\alpha}{r_0} + \ln(r_0) - 1, \tag{27}$$

which satisfies the conditions for $h(r_\alpha)$.

The time derivative of V_1 is now

$$\dot{V}_1 = v_1 \tan(\phi) \left[u \left(1 - \frac{r_\alpha \kappa}{\cos(\phi)} + f(r_\alpha)r_\alpha \right) - \frac{\kappa}{\cos(\phi)} + f(r_\alpha) \right], \tag{28}$$

where we have used Eqs. 23, 24, and 25. We now assume that the speed $v_1 > 0$ is a constant and design steering control u so that $\dot{V}_1 \leq 0$.

3.2 Tracking Control for Convex Curves

We first consider the case when the curve is convex and curving away from the vehicle. In this case, we have $\kappa < 0$.

One choice of u that leads to $\dot{V}_1 \leq 0$ is

$$u_1 = \frac{v_1 \kappa - \cos(\phi)(v_1 f(r_\alpha) + \mu \sin(\phi))}{v_1(\cos(\phi) + f(r_\alpha)r_\alpha \cos(\phi) - r_\alpha \kappa)}, \tag{29}$$

where $\mu > 0$ is a constant. The time derivative of V_1 in Eq. 28 with u given by Eq. 29 is

$$\dot{V}_1 = -\mu \frac{\sin^2(\phi)}{\cos(\phi)} \leq 0, \tag{30}$$

where Eq. 3 is used. Thus, $\dot{V}_1 \leq 0$ and $\dot{V}_1 = 0$ if and only if $\sin(\phi) = 0$. However, by Eq. 3, we see that $\dot{V}_1 = 0$ if and only if $\phi = 0$.

From now on, we refer to the case where the denominator of a control law is zero as the *singular case* of the controller. It seems possible that the control law given by Eq. 29 is singular when $\cos(\phi) = \frac{r_\alpha \kappa}{1 + f(r_\alpha)r_\alpha}$. Using Eq. 26, we have

$$\cos(\phi) = \frac{r_\alpha \kappa}{1 + f(r_\alpha)r_\alpha} = r_0 \kappa. \tag{31}$$

Therefore, in the case where the curvature of the lane at the *detected point* κ is equal to or smaller than zero in Eq. 31, the denominator of the control law in Eq. 29 will never be zero since $\cos(\phi) > 0$.

Theorem 1 Consider the case where the boundary curve is convex, i.e., $\kappa < 0$. Then, using the steering control law in Eq. 29, the vehicle satisfying Eq. 3 with constant speed $v_1 > 0$ tracks the curve at a distance r_0 without collision.

Proof For each trajectory that initially satisfies Eq. 3 and $r_\alpha > 0$, there exists a compact sublevel set Ω of V_1 such that the trajectory remains in Ω for all future time. Then, by LaSalle’s Invariance Principle [34], the trajectory converges to the largest invariant set M within the set E that contains all points in Ω where $\dot{V}_1 = 0$. The set E in this case is the set of all points in Ω such that $\phi = 0$. Note that $\phi = 0$ implies $\dot{r}_\alpha = 0$ using Eq. 23. Thus, at any point in E , the dynamics may be expressed as

$$\dot{r}_\alpha = 0. \tag{32}$$

Since the trajectory converges to the maximum invariant set M within the set E where $\phi = 0$, then $\dot{\phi} \rightarrow 0$. Therefore, replacing the term $\dot{\phi}$ in Eq. 24 by 0 gives

$$v_1 u_1 - v_1 (r_\alpha u_1 + 1) \kappa = 0. \tag{33}$$

On the set E , the control input u_1 is

$$u_1 = \frac{\kappa}{1 - r_\alpha \kappa}. \tag{34}$$

When we substitute ϕ in Eq. 29 for 0, the corresponding control input is

$$u_1 = \frac{\kappa - f(r_\alpha)}{1 + f(r_\alpha)r_\alpha - r_\alpha \kappa}. \tag{35}$$

u_1 in Eq. 35 should be equal to u_1 in Eq. 34, because both u_1 are control inputs on the invariant set. Thus, we obtain

$$\frac{\kappa}{1 - r_\alpha \kappa} = \frac{\kappa - f(r_\alpha)}{1 + f(r_\alpha)r_\alpha - r_\alpha \kappa}, \tag{36}$$

which implies

$$(\kappa - f(r_\alpha))(1 - r_\alpha \kappa) = \kappa + f(r_\alpha)r_\alpha \kappa - r_\alpha \kappa^2. \tag{37}$$

Therefore, $f(r_\alpha)$ must satisfy

$$f(r_\alpha) = 0. \tag{38}$$

The moving vehicle converges to the position at a distance from the boundary curve given by the zero of the function $f(\cdot)$. Therefore, the largest invariant set contained in E may be expressed as

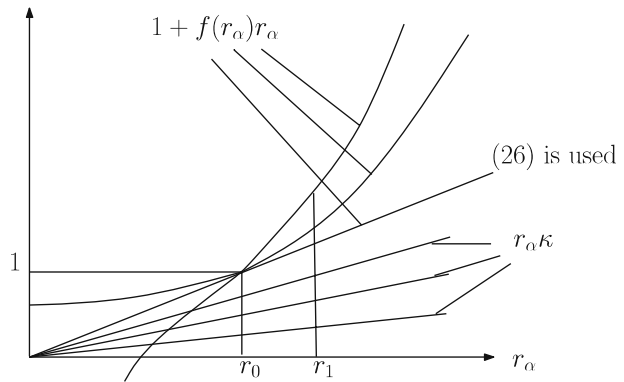
$$M = \{(r_\alpha, \phi) | \phi = 0, f(r_\alpha) = 0\}. \tag{39}$$

Thus, we can conclude that (r_α, ϕ) converges to the equilibrium where $r_\alpha = r_0$ and $\phi = 0$. □

3.3 Control Laws for Concave Curve with Bounded Curvature

We consider the case when the curve is concave, i.e., curving towards the vehicle. In this case, we have $\kappa > 0$. It is possible that the control law given by Eq. 29 is singular

Fig. 3 Comparison of $1 + f(r_\alpha)r_\alpha$ and $r_\alpha\kappa$. Control law given by Eq. 29 is singular when $\cos(\phi) = \frac{r_\alpha\kappa}{1+f(r_\alpha)r_\alpha}$. We argue that singular case cannot be removed by choosing $f(r_\alpha)$ if the curvature κ is upper bounded



when the denominator of u_1 equals zero, i.e., $\cos(\phi) = \frac{r_\alpha\kappa}{1+f(r_\alpha)r_\alpha}$. However, in the case where the curvature of the lane at the detected point κ is bigger than $\frac{1}{r_0}$ in Eq. 31, no singularity happens because $|\cos \phi| \leq 1$.

In the real experimental environment, it is necessary for the vehicle to follow a concave curve whose curvature is small. We argue that, in this case, singularity exists regardless of the choice of $f(r_\alpha)$. Figure 3 shows possible graphs of $1 + f(r_\alpha)r_\alpha$ and $r_\alpha\kappa$, respectively. When Eq. 26 is used as $f(r_\alpha)$, we get $1 + f(r_\alpha)r_\alpha = \frac{r_\alpha}{r_0}$. Therefore, the straight line connecting the origin and $(r_0, 1)$ represents $1 + f(r_\alpha)r_\alpha$ when Eq. 26 is used as $f(r_\alpha)$. In Fig. 3, regardless of $f(r_\alpha)$, $1 + f(r_\alpha)r_\alpha$ is a continuous function that is equal to 1 when $r_\alpha = r_0$. Also, regardless of the decreasing rate of $f(r_\alpha)$ as $r_\alpha \rightarrow 0$, we can assure that $\lim_{r_\alpha \rightarrow 0} 1 + f(r_\alpha)r_\alpha \leq 1$. As $r_\alpha \downarrow r_0$, we see that $f(r_\alpha)$ and r_α both decrease to make $(1 + f(r_\alpha)r_\alpha)$ decrease for any choice of $f(r_\alpha)$. Meanwhile, the possible $r_\alpha\kappa$ are plotted as the straight lines. If the curvature κ is upper bounded by $\frac{1}{r_0}$, then these straight lines will be below the curve that represents $(1 + f(r_\alpha)r_\alpha)$, regardless of what $f(r_\alpha)$ is. Therefore, $\frac{r_\alpha\kappa}{1+f(r_\alpha)r_\alpha} < 1$ and $\cos \phi = \frac{r_\alpha\kappa}{1+f(r_\alpha)r_\alpha}$ always have a solution for ϕ . This singularity cannot be removed by changing $f(r_\alpha)$.

3.4 The Safety Zone

Due to Eq. 31, if $|\phi| < \arccos(r_0\kappa_M)$, where κ_M is the upper bound of κ , then $\cos \phi > r_0\kappa$ implies that the singular case will never happen. Thus, we define the set

$$U = \{(r_\alpha, \phi) | V_1(r_\alpha, \phi) < -\ln(|r_0\kappa_M|)\} \tag{40}$$

as the *safety zone*. Note that we assume $\kappa_M r_0 < 1$ since, otherwise, the desired distance is too far away from the curve, which makes tracking meaningless. The controller Eq. 29 is used inside the safety zone. Since this controller yields $\dot{V}_1 \leq 0$, we conclude that, once the vehicle under control enters the safety zone U , it will never leave. Therefore, according to Theorem 1, the curve tracking behavior is stabilized without collision if the vehicle starts *inside* the safety zone.

3.5 Switching Control that Aims for the Safety Zone

When the vehicle is initially out of the safety zone but, during its movements, it will come close to the set where $\cos(\phi) = r_0\kappa$, control law Eq. 29 cannot be applied due to singularity. The singular cases when $\sin(\phi) < 0$ are plotted in Fig. 4. The singularities occur when the vehicle is positioned on the line l , and the angle ϕ satisfies $\cos(\phi) = r_0\kappa$. The angle $\phi < 0$ is measured counterclockwise from \vec{x}_2 at the detected point p to the heading direction of the vehicle \vec{x}_1 . Hence, when $\phi > 0$, the vehicle will be at the same position but heading away from the boundary curve. In Fig. 4, r_k denotes the radius of the osculating circle at the point p so that $r_k = 1/\kappa$. The vehicle's desired curve is plotted as d that has r_0 distance from the boundary curve. In the illustrated case, the controller design problem should be reconsidered because the goal of the controller now is to steer into the safety zone. Intuitively, this means to steer away from the boundary curve promptly, which is a natural behavior when we drive our cars on a collision course to a concave wall. Therefore, we now design controllers so that the vehicle enters the safety zone U in finite time.

We develop a switching system as depicted in Fig. 5 to steer the system into the safety zone in finite time. Four cases are distinguished, which correspond to four sets G_1, G_2, G_3 , and G_4 defined as follows:

$$\begin{aligned}
 G_1 &= \{(r_\alpha, \phi) \mid \|\cos(\phi) - r_0\kappa\| > \epsilon \text{ but } (r_\alpha, \phi) \notin U\} \\
 G_2 &= \{(r_\alpha, \phi) \mid \epsilon_2 < \|\cos(\phi) - r_0\kappa\| \leq \epsilon\} \\
 G_3 &= \{(r_\alpha, \phi) \mid \|\cos(\phi) - r_0\kappa\| \leq \epsilon_2\} \\
 G_4 &= U,
 \end{aligned} \tag{41}$$

where $\epsilon_2 < \epsilon$.

Three control laws are designed for these four cases. When the system states are in G_1 or G_4 , we use u_1 in Eq. 29. When the states enter G_2 from G_1 , we switch to u_2 , which is

$$u_2 = \frac{v_1\kappa - \cos(\phi)(v_1 f(r_\alpha) + \mu_2 \sin(\phi))}{v_1(\cos(\phi) + f(r_\alpha)r_\alpha \cos(\phi) - r_\alpha\kappa)}, \tag{42}$$

Fig. 4 The positions of a vehicle when singularities occur and $\phi < 0$. Here, the vehicle's desired curve is plotted as d that has r_0 distance from the boundary curve. The singularities occur when the vehicle is positioned on the line l , and the angle ϕ satisfies $\cos(\phi) = r_0\kappa$

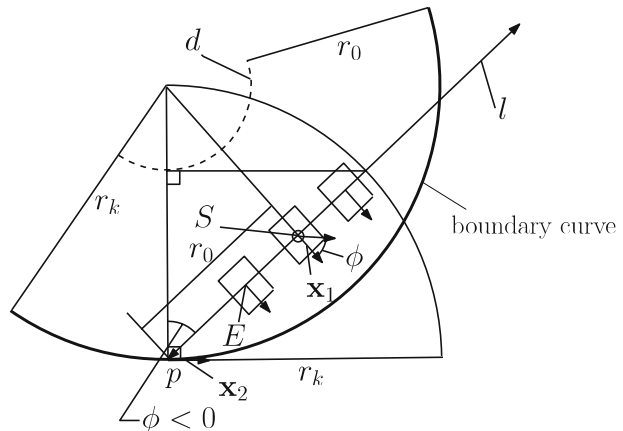
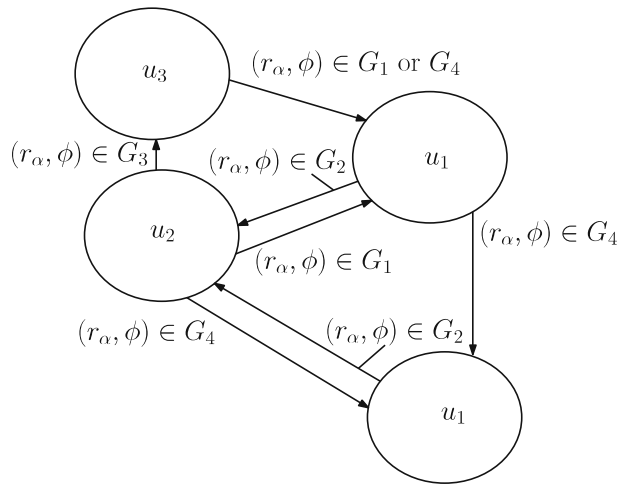


Fig. 5 The switching control strategy used to enter the safety zone. u_1 in Eq. 29 is used in normal situations, i.e., when the states are in G_1 or G_4 . We switch to u_2 in Eq. 42 when the states enter G_2 and switch to u_3 in Eq. 44 when the states enter G_3



u_1	$u_1 = \frac{r_1 \kappa - \cos(\phi)(v_1 f(r_\alpha) + \mu \sin(\phi))}{v_1(\cos(\phi) + f(r_\alpha)r_\alpha \cos(\phi) - r_\alpha \kappa)}$
u_2	$u_2 = \frac{r_1 \kappa - \cos(\phi)(v_1 f(r_\alpha) + \mu_2 \sin(\phi))}{v_1(\cos(\phi) + f(r_\alpha)r_\alpha \cos(\phi) - r_\alpha \kappa)}$
u_3	$u_3 = \frac{-\mu_3 \sin(\phi) + \kappa v_1 r_\alpha}{v_1 r_\alpha (\cos(\phi) - r_\alpha \kappa)}$

where the only difference between u_1 and u_2 is that μ_2 is much bigger than μ . The time derivative of V_1 under control u given by Eq. 42 is

$$\dot{V}_1 = -\mu_2 \frac{\sin^2(\phi)}{\cos(\phi)} \leq 0. \tag{43}$$

When the states of the system enter G_3 from G_2 , we switch to controller u_3 :

$$u_3 = \frac{-\mu_3 \sin(\phi) + \kappa v_1 r_\alpha}{v_1 r_\alpha (\cos(\phi) - r_\alpha \kappa)}, \tag{44}$$

where $\mu_3 > 0$ is a constant. Under this controller, we have

$$\dot{\phi} = -\frac{\mu_3 \tan(\phi)}{r_\alpha}. \tag{45}$$

Hence, $\phi \rightarrow 0$ as $t \rightarrow \infty$. This implies that the system states will get out of G_3 and then out of G_2 in finite time. We switch back to controller u_1 after the states enter either G_1 or G_4 . Note that, by Theorem 1, once the states enter G_4 , they will stay in G_4 and converge to the desired values.

We now prove convergence of the system under the switching control laws illustrated in Fig. 5. The idea is that the value of the Lyapunov function V_1 may be increasing under controller u_3 , but such increase will be compensated by controller u_2 . Hence, the overall effect is that the Lyapunov function decreases until the system reaches G_4 . Some notations and technical conditions are needed to rigorously state and prove the results.

It is uninteresting if the states never enter the set G_3 . In this case, V_1 would be decreasing until G_4 is reached. Therefore, we discuss the most general case, i.e., the states of the system enter G_3 for a number of times. In order to enter G_3 , the system must enter G_2 first. We use the notations t_1^i to indicate the time when the system enters G_2 , t_2^i to indicate the time when the system enters G_3 , and t_3^i to indicate the time when the system leaves G_2 . The index i is used to distinguish multiple entries. If the states enter G_3 and later leave G_2 , then $t_1^i, t_2^i,$ and t_3^i happen in sequence.

The following technical assumptions are needed:

- (A1) The curvature κ is bounded above by $\kappa_M > 0$.
- (A2) The desired distance r_0 satisfies that $r_0\kappa_M < 1$.
- (A3) Define

$$\zeta = v_1 \| -\arccos(\kappa_M r_0 + \epsilon) + \arccos(\kappa_M r_0 - \epsilon_2) \| + \epsilon_3,$$

where $\epsilon_3 > 0$ is a constant. The gain μ_2 and μ_3 in controllers u_2 and u_3 satisfy $\mu_2\mu_3(t_2^i - t_1^i) > \frac{\zeta r_0 \kappa_M}{1 - (r_0 \kappa_M)^2}$ for all i .

Assumptions A1 and A2 put mild constraints on the curve to follow. Assumption A3 is the key technical assumption. This assumption is satisfied when $t_2^i - t_1^i \neq 0$ and if we use sufficiently large gains μ_2 or μ_3 .

Theorem 2 Consider the system defined by Eqs. 23 and 24 governing the relative distance and heading angle between the vehicle and the detected point. Suppose the vehicle travels at constant speed v_1 . Under the switching strategy in Fig. 5, with assumptions A1–A3 satisfied, the states of the closed loop system enter G_4 in finite time.

Proof We organize our proofs in two steps:

1. Show that, when u_3 is used, V_1 will increase a finite amount bounded above.
2. Show that, when u_2 is used, V_1 will decrease more than the upper bound for its increase under u_3 .

1. Estimate the upper bound for the increase of V_1 under u_3 .

The time derivative of V_1 under u_3 is

$$\dot{V}_1 = -\tan(\phi) \left[u_3 \left(\frac{v_1 r_\alpha \kappa}{\cos(\phi)} - v_1 \frac{r_\alpha}{r_0} \right) + \frac{v_1}{\cos(\phi)} \kappa - v_1 \left(\frac{-1}{r_\alpha} + \frac{1}{r_0} \right) \right], \tag{46}$$

where Eq. 26 is used as $f(r_\alpha)$. Notice that u_3 is used only in the small neighborhood of $\cos(\phi) = \kappa r_0$. Replacing $\cos(\phi)$ in Eq. 46 by κr_0 , we get

$$\dot{V}_1 = -\tan(\phi) \frac{v_1}{r_\alpha}. \tag{47}$$

If $\sin(\phi) \geq 0$, then $\dot{V}_1 \leq 0$ is guaranteed. This implies that V_1 decreases while u_3 is used. This case is uninteresting.

The case that V_1 may increase is shown in Fig. 4. We now estimate the increase of V_1 while u_3 is used as the control law.

$$V_1(t_3^i) - V_1(t_2^i) = -v_1 \int_{t_2^i}^{t_3^i} \frac{\tan(\phi(t))}{r_\alpha(t)} dt. \tag{48}$$

We can change Eq. 48 to integration with respect to ϕ as

$$V_1(t_3^i) - V_1(t_2^i) = \frac{v_1}{\mu_3} \int_{\phi(t_2^i)}^{\phi(t_3^i)} d\phi = \frac{v_1}{\mu_3} (\phi(t_3^i) - \phi(t_2^i)), \tag{49}$$

where Eq. 45 is used. The controller u_3 is applied from the instant when $|\cos(\phi) - \kappa r_0| = \epsilon_2$ to the instant when $|\cos(\phi) - \kappa r_0| = \epsilon$, where $\epsilon_2 < \epsilon$. Therefore, we get $|\cos(\phi(t_2^i)) - \kappa r_0| = \epsilon_2$ and $|\cos(\phi(t_3^i)) - \kappa r_0| = \epsilon$. Thus, when $\phi < 0$, possible values of ϕ can be listed as follows:

$$\begin{aligned} \phi(t_2^i) &= -\arccos(\kappa r_0 \pm \epsilon_2) < 0 \\ \phi(t_3^i) &= -\arccos(\kappa r_0 \pm \epsilon) < 0. \end{aligned} \tag{50}$$

We plot these possible values on Fig. 6. Within the interval of $-\pi/2 < \phi < 0$, $\cos(\phi)$ increases as ϕ increases. Thus, we get $-\arccos(\kappa r_0 + \epsilon) > -\arccos(\kappa r_0 - \epsilon)$, and $-\arccos(\kappa r_0 + \epsilon_2) > -\arccos(\kappa r_0 - \epsilon_2)$. Therefore, we conclude that

$$\begin{aligned} \phi(t_3^i) - \phi(t_2^i) &\leq \max(\phi(t_3^i)) - \min(\phi(t_2^i)) \\ &= -\arccos(\kappa r_0 + \epsilon) \\ &\quad + \arccos(\kappa r_0 - \epsilon_2). \end{aligned} \tag{51}$$

Figure 6 compares between

$$-\arccos(\kappa r_0 + \epsilon) + \arccos(\kappa r_0 - \epsilon_2)$$

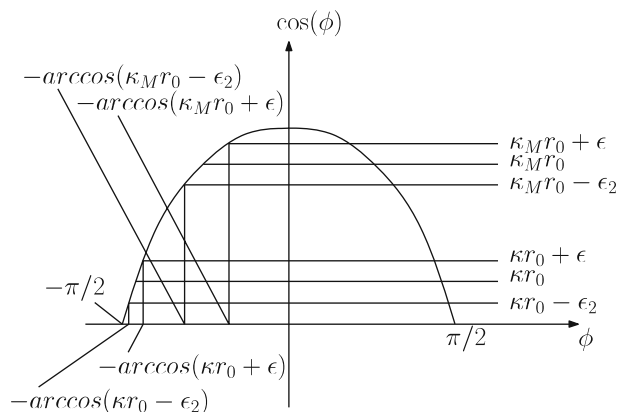
and

$$-\arccos(\kappa_M r_0 + \epsilon) + \arccos(\kappa_M r_0 - \epsilon_2).$$

The slope of $\cos(\phi)$ with respect to ϕ is $\frac{d\cos(\phi)}{d\phi} = -\sin(\phi)$. It monotonously decreases to zero as ϕ goes to zero in the interval of $-\pi/2 < \phi < 0$. Thus, as seen in Fig. 6, we get

$$\begin{aligned} &-\arccos(\kappa r_0 + \epsilon) + \arccos(\kappa r_0 - \epsilon_2) \\ &\leq -\arccos(\kappa_M r_0 + \epsilon) + \arccos(\kappa_M r_0 - \epsilon_2). \end{aligned}$$

Fig. 6 Comparison of $-\arccos(\kappa r_0 + \epsilon) + \arccos(\kappa r_0 - \epsilon_2)$ and $-\arccos(\kappa_M r_0 + \epsilon) + \arccos(\kappa_M r_0 - \epsilon_2)$. The slope of $\cos(\phi)$ with respect to ϕ , which is $\frac{d\cos(\phi)}{d\phi} = -\sin(\phi)$, monotonously decreases to zero as ϕ goes to zero in the interval of $-\pi/2 < \phi < 0$. Therefore, as seen on this figure, we get $-\arccos(\kappa r_0 + \epsilon) + \arccos(\kappa r_0 - \epsilon_2) \leq -\arccos(\kappa_M r_0 + \epsilon) + \arccos(\kappa_M r_0 - \epsilon_2)$



According to Eq. 51, we deduce that

$$\phi(t_3^i) - \phi(t_2^i) \leq -\arccos(\kappa_M r_0 + \epsilon) + \arccos(\kappa_M r_0 - \epsilon_2). \tag{52}$$

Now, using Eqs. 49 and 52, we can derive the upper bound for the increase of V_1 while u_3 is used.

$$V_1(t_3^i) - V_1(t_2^i) \leq \frac{v_1}{\mu_3} (-\arccos(\kappa_M r_0 + \epsilon) + \arccos(\kappa_M r_0 - \epsilon_2)) < \frac{\zeta}{\mu_3}, \tag{53}$$

where ζ is defined in assumption A3.

2. We show that, under assumption A3, the decrease of V_1 under u_2 is larger than the upper bound of the increase of V_1 under u_3 .

We compute the required length of the time interval when u_2 is used so that V_1 decreases more than ζ/μ_3 . In other words,

$$V_1(t_2^i) - V_1(t_1^i) = \int_{t_1^i}^{t_2^i} \dot{V}_1 dt < -\frac{\zeta}{\mu_3}, \tag{54}$$

where t_1^i and t_2^i represent the beginning and the end of the interval when u_2 is used, respectively. Hence, using Eq. 43, we require that

$$\int_{t_1^i}^{t_2^i} \frac{\mu_2 \sin^2(\phi)}{\cos(\phi)} dt = (t_2^i - t_1^i) \frac{\mu_2 \sin^2(\phi(\tau))}{\cos(\phi(\tau))} > \frac{\zeta}{\mu_3}, \tag{55}$$

where $\tau \in [t_1^i, t_2^i]$ and the mean value theorem are applied. Further, we get the required length of the interval when u_2 is used so that V_1 decreases more than ζ/μ_3 as

$$(t_2^i - t_1^i) > \frac{\zeta \cos(\phi(\tau))}{\mu_2 \mu_3 \sin^2(\phi(\tau))}. \tag{56}$$

As seen in Fig. 5, u_2 is used in the near-singular state. Thus, we can see that $\cos(\phi(\tau)) \approx r_0 \kappa \leq r_0 \kappa_M < 1$ using assumption A2. Therefore, we get

$$\begin{aligned} \frac{\sin^2(\phi(\tau))}{\cos(\phi(\tau))} &= \frac{1}{\cos(\phi(\tau))} - \cos(\phi(\tau)) \\ &\geq \frac{1}{r_0 \kappa_M} - r_0 \kappa_M > 0. \end{aligned} \tag{57}$$

This is equivalent to

$$\frac{\cos(\phi(\tau))}{\sin^2(\phi(\tau))} \leq \frac{r_0 \kappa_M}{(1 - (r_0 \kappa_M)^2)}. \tag{58}$$

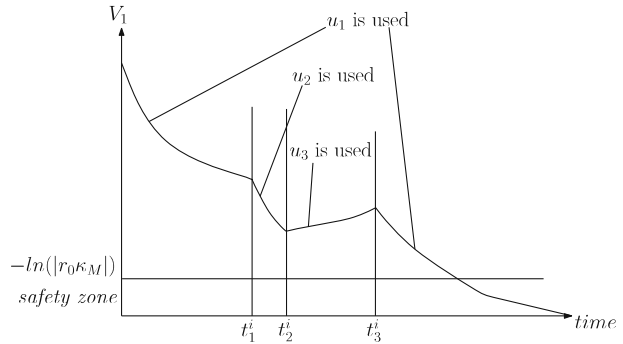
Multiplying both sides of Eq. 58 by $\frac{\zeta}{\mu_2 \mu_3}$, we derive

$$\frac{\zeta \cos(\phi(\tau))}{\mu_2 \mu_3 \sin^2(\phi(\tau))} \leq \frac{\zeta r_0 \kappa_M}{\mu_2 \mu_3 (1 - (r_0 \kappa_M)^2)}. \tag{59}$$

Therefore, using Eqs. 56 and 59, if

$$(t_2^i - t_1^i) > \frac{\zeta r_0 \kappa_M}{\mu_2 \mu_3 (1 - (r_0 \kappa_M)^2)}, \tag{60}$$

Fig. 7 Lyapunov function V_1 in a typical case of switching control. u_1 in Eq. 29 is used from 0 to t_1^i , u_2 in Eq. 42 is used from t_1^i to t_2^i , u_3 in Eq. 44 is used from t_2^i to t_3^i , and u_1 is used from t_3^i to final time



we can guarantee that the decrease of V_1 under controller u_2 is greater than the increase of V_1 under controller u_3 by an amount of ϵ_3/μ_3 . We can then conclude that switching among u_1 , u_2 , and u_3 will make the system enter the safety zone in finite time. □

In Fig. 7, a typical switching process is plotted. Controller u_1 is used from 0 to t_1^i , u_2 is used from t_1^i to t_2^i , u_3 is used from t_2^i to t_3^i , and u_1 is used again after t_3^i . In assumption A3, we used arbitrarily large μ_2 or μ_3 so that the interval of using u_2 is long enough to overcome the increase of V_1 inside the interval when u_3 is used. Therefore, V_1 always decreases more than it increases.

In the case where $r_\alpha = r_0$ and $\cos(\phi) = r_0\kappa$, we have singular cases of u_1 , u_2 , and u_3 at the same time. This is the *common singular case* that occurs when the vehicle is at point S in Fig. 4. As seen in Fig. 4, the heading direction \vec{x}_1 of the vehicle at S is normal to the desired curve d . This singular case will not happen if the vehicle is in the safety zone. Since it happens only at point S and the vehicle has constant speed, we conclude that the vehicle will not likely be in this state unless it starts initially in this state. The authors of [2] also mentioned that the moving vehicle should not be initially heading directly toward the boundary curve when control laws based on closest point information are applied.

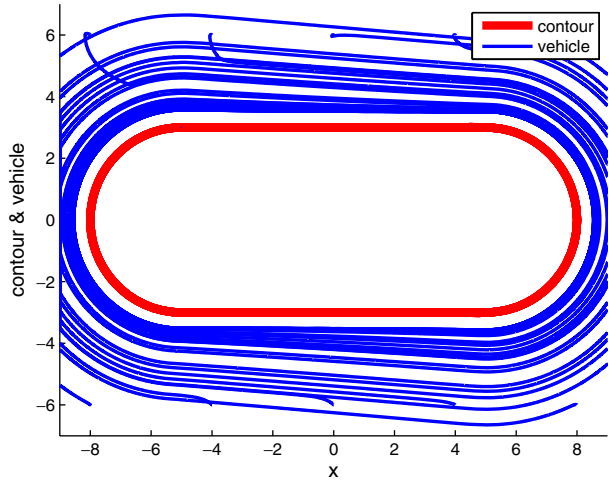
4 Simulation Results

We implement our feedback control law in MATLAB, as well as in the three-dimensional simulation program used in the Georgia Tech urban grand challenge system. Our three-dimensional simulation program is based on Player, Stage, and Gazebo, which are three pieces of software developed for robotic simulation projects. We simulate the case that a vehicle tracks a boundary curve in the clockwise direction.

4.1 MATLAB Simulation Results

Figure 8 shows a vehicle following a closed boundary curve in a clockwise direction starting from multiple initial conditions. We vary the vehicle’s initial x coordinate from -8 to 8 , and y coordinate from -6 to 6 , with initial orientation $3\pi/4$ measured

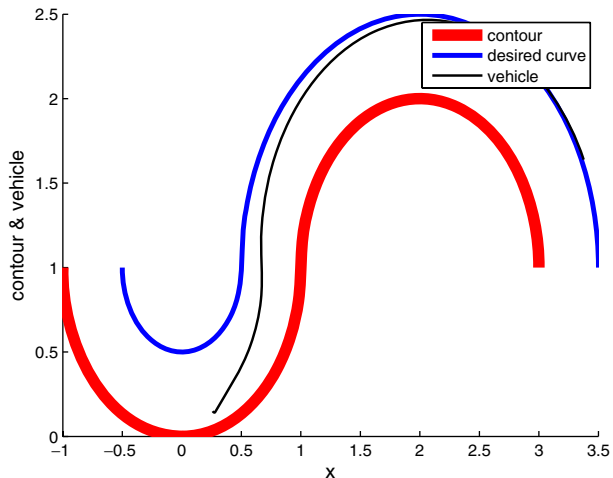
Fig. 8 MATLAB simulation result showing clockwise circling of a lane-shaped curve starting from multiple initial conditions. We vary the vehicle’s initial x coordinate from -8 to 8 , and y coordinate from -6 to 6 , with initial orientation $3\pi/4$ measured counterclockwise from the x axis



counterclockwise from the x axis. The desired separation between the vehicle and the boundary curve is set to 0.5 distance unit, and velocity of the vehicle v_1 is 0.5 distance unit per unit time.

Figure 9 is a simulation showing the result of using the switched controller to overcome singularity. In order to compare with Fig. 4, the vehicle moves toward a concave curve initially, the curvature of which is 1. Also, the desired curve has 0.5 distance unit from the obstacle. Initial position and heading angle of a vehicle are the same as the vehicle’s position E in Fig. 4. We can find that, using this switched controller strategy, the autonomous vehicle converges to the desired curve very smoothly, as expected.

Fig. 9 MATLAB simulation showing the result of using the switched controller to overcome singularity. The initial position and heading angle of the vehicle are the same as the vehicle’s position E in Fig. 4. Switching occurs at the near-singular case, and the vehicle is steered away from the boundary curve promptly



4.2 Results Using the Three-Dimensional Simulation Program

Our feedback control law is verified using the three-dimensional simulation program developed for the Georgia Tech urban grand challenge system. To estimate the curvature at the detected point using a group of rays around the center ray, we use the following estimation method.

Let P_n represent the detected point. Further, P_{n-w}, P_{n+w} denote two points on the boundary curve detected using two rays around the center ray with window size w . Estimate of curvature was proposed in [35] as follows. Let $a = \|P_n - P_{n-w}\|$, $b = \|P_{n+w} - P_n\|$, $c = \|P_{n+w} - P_{n-w}\|$, and $s = (a + b + c)/2$. We draw the unique circle passing all three points. By applying Heron’s formula, the curvature of such a circle is

$$\|\hat{\kappa}(s)\| = \frac{4\sqrt{s(s-a)(s-b)(s-c)}}{abc}. \tag{61}$$

In [35], it was proved that $\hat{\kappa}$ is a good estimate of κ when the difference $(a - b)$ is sufficiently small. We refer to this estimate as the *geometric estimate* of curvature. In [3], the authors derived the extended version of this geometric curvature estimate. For example,

$$\bar{\kappa}(n) = \frac{1}{3} \sum_{w=7}^9 \hat{\kappa}(P_{n-w}, P_n, P_{n+w}), \tag{62}$$

where $\hat{\kappa}(P_{n-w}, P_n, P_{n+w})$ denotes the geometric estimate of curvature obtained at the P_n with window size w . In [3], it was shown that using a larger window size eliminates the need for Gaussian filtering. In our simulation experiment, Eq. 62 is taken as a method to estimate the curvature of the lane at the detected point P_n .

Figures 10, 11, 12, 13, 14 show the simulation results using this three-dimensional simulation program. The desired distance r_0 is set to 10 distance units, and the vehicle’s velocity v_1 is set to six distance units per second.

In Fig. 10, on the right side of the initial position of the vehicle, we constructed a cylinder-shaped obstacle. The diameter and the height of the obstacle are set to 40 distance units and 20 distance units, respectively. Figure 11 shows that the vehicle converges to the position where the relative distance from the obstacle r_α is almost 10 distance units, as we desired. Figure 12 shows that r_α converges to the desired r_0 .

Fig. 10 Initial position of the vehicle in the three-dimensional simulation. On the right side of the vehicle, we can find a cylinder-shaped obstacle. The diameter and the height of the obstacle are set to 40 distance units and 20 distance units, respectively

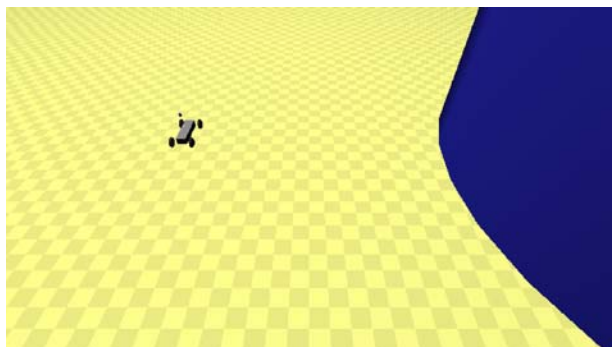


Fig. 11 Final position of the vehicle in the three-dimensional simulation. The vehicle converges to the position where the relative distance from the obstacle (r_α) is almost 10 distance units, as we desired

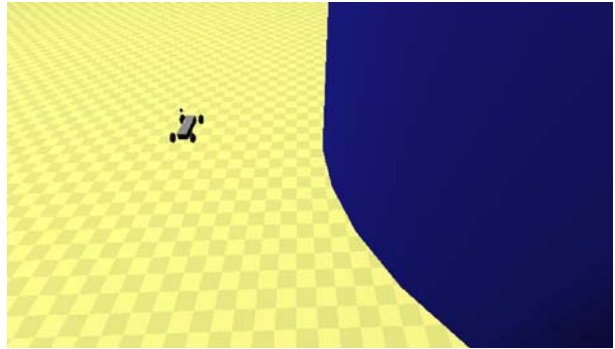


Fig. 12 The vehicle's relative distance (r_α) with respect to time

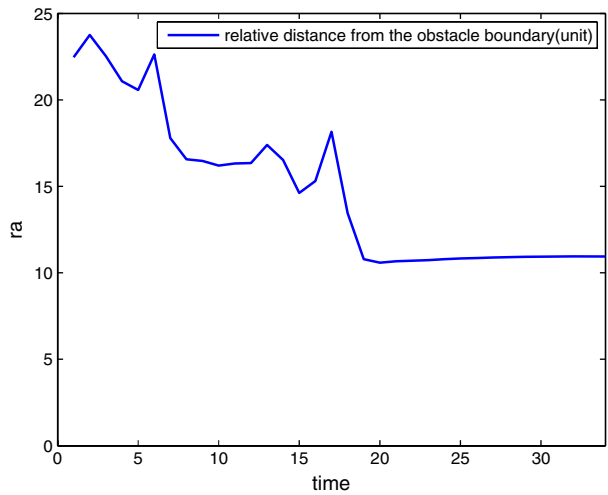


Fig. 13 The vehicle's relative heading angle (ϕ) converges to almost 0 as time goes on

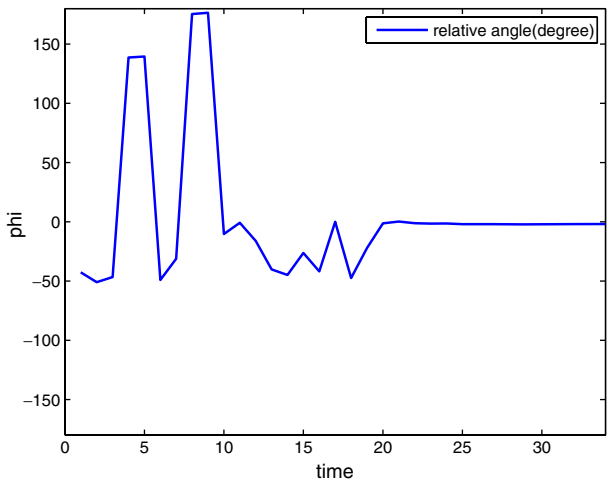


Fig. 14 Displayed values on the control panel of the simulation at ending time. The desired distance (r_0) is set to 10 distance units, and the vehicle’s velocity (v_1) is set to six distance units per second. Accordingly, we can see relative distance ($r_\alpha = 10.0$ distance units), relative angle ($\phi = -1.0$ degree), and vehicle speed ($v_1 = 6.0$ distance units per second) on the left side of this control panel. On the right side of the panel, the planar trajectory of the vehicle is displayed as a *circle*, since we have a cylinder-shaped obstacle

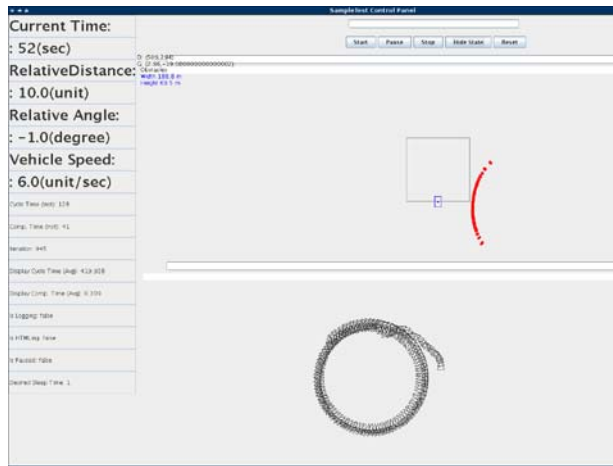


Figure 13 shows that the vehicle’s relative heading angle ϕ converges to 0 as time goes on. The overshoot of the initial relative heading angle is large since switched control laws are used to overcome the singularity caused by the error in the curvature estimate using Eq. 62. Figure 14 displays the values on the control panel at the ending time. On the right side of the panel, the trajectory of the vehicle projected to the plane is displayed.

5 Summary and Future Work

In this paper, we design a curve tracking control law that uses information from rigidly mounted, narrow-aperture-range sensors. The key idea is to control the relative motion between the vehicle and the detected point and to switch controllers to prevent singularities.

Several improvements of the current control strategy can be expected. Since we have derived the tracking model for mounting angle α , an extension for the controller from $\alpha = \pi/2$ to the general case is underway. We estimate the curvature of the curve at the detected point based on range measurements. We observe from simulation that such estimate contains noise that may cause unnecessary switching that affects the tracking performance. Hence, a filtering algorithm for curvature estimation can be developed to reduce the noise. In addition, multiple vehicles with rigidly mounted sensors can be coordinated, similar to [36] and [37], for dynamic boundary estimation.

Acknowledgements This research is supported by ONR grant N00014-08-1-1007 and NSF grant ECCS-0841195. We thank Matt Powers for his assistance in working on the three-dimensional simulation program used in the Georgia Tech urban grand challenge system.

References

1. Egerstedt, M., Hu, X., Stotsky, A.: Control of mobile platforms using a virtual vehicle approach. *IEEE Trans. Automat. Contr.* **46**, 1777–1782 (2001)
2. Zhang, F., Justh, E., Krishnaprasad, P.S.: Boundary following using gyroscopic control. In: Proc. of 43rd IEEE Conf. on Decision and Control, pp. 5204–5209, Atlantis, 14–17 December 2004
3. Zhang, F., O'Connor, A., Luebke, D., Krishnaprasad, P.S.: Experimental study of curvature-based control laws for obstacle avoidance. In: Proc. of IEEE International Conf. on Robotics and Automation, pp. 3849–3854, New Orleans, 24–27 April 2004
4. Zhang, F., Leonard, N.E.: Coordinated patterns of unit speed particles on a closed curve. *Syst. Control. Lett.* **56**, 397–407 (2007)
5. Zhang, F., Fiorelli, E., Leonard, N.E.: Exploring scalar fields using multiple sensor platforms: tracking level curves. In: Proc. of 46th IEEE Conf. on Decision and Control, pp. 3579–3584, New Orleans, 12–14 December 2007
6. Zhang, F., Fratantoni, D.M., Paley, D., Lund, J., Leonard, N.E.: Control of coordinated patterns for ocean sampling. *Int. J. Control* **80**, 1186–1199 (2007)
7. Reddy, P.V., Justh, E.W., Krishnaprasad, P.: Motion camouflage in three dimensions. In: Proc. of 45th IEEE Conf. on Decision and Control, pp. 3327–3332, San Diego, 13–15 December 2006
8. Justh, E.W., Krishnaprasad, P.S.: Natural frames and interacting particles in three dimensions. In: Proc. of 44th IEEE Conf. on Decision and Control, pp. 2841–2846, Seville, 12–15 December 2005
9. Samson, C.: Control of chained systems: application to path-following and time-varying point-stabilization of mobile robots. *IEEE Trans. Automat. Contr.* **40**, 64–77 (1995)
10. Frezza, R., Picci, G.: On line path following by recursive spline updating. In: Proc. of 34th IEEE Conf. on Decision and Control, pp. 4047–4052, New Orleans, 13–15 December 1995
11. Ma, Y., Koseck'a, J., Sastry, S.: Vision guided navigation for a nonholonomic mobile robot. In: Proc. of 36th IEEE Conference on Decision and Control, pp. 3069–3074, San Diego, 10–12 December 1997
12. Justh, E.W., Krishnaprasad, P.S.: Steering laws for motion camouflage. *R. Soc. Lond. Proc. Ser. A* **462**, 3629–3643 (2006)
13. Li, K., Baillieul, J.: Data-rate requirements for nonlinear feedback control. In: Proc. of 6th IFAC Symp. Nonlinear Contr. Sys., pp. 1277–1282, Stuttgart, 1–3 September 2004
14. Micaelli, A., Samson, C.: Trajectory tracking for unicycle-type and two-steering-wheels mobile robots. INRIA, Tech. Rep. (1993)
15. Andersson, S.B., Park, J.: Tip steering for fast imaging in AFM. In: Proc. of American Control Conference, pp. 2469–2474, Portland, 8–10 June 2005
16. Clark, J., Fierro, R.: Cooperative hybrid control of robotic sensors for perimeter detection and tracking. In: Proc. of American Control Conference, pp. 3500–3505, Portland, 8–10 June 2005
17. Corke, P., Detweiler, C., Dunbabin, M., Hamilton, M., Rus, D., Vasilescu, I.: Experiments with underwater robot localization and tracking. In: Proc. of IEEE International Conference on Robotics and Automation, pp. 4556–4561, Roma, 10–14 April 2007
18. Carmo, M.D.: *Differential Geometry of Curves and Surfaces*. Prentice Hall, Englewood Cliffs (1976)
19. Dickmanns, E.D., Graefe, V.: Applications of dynamic monocular machine vision. *Mach. Vis. Appl.* **1**, 241–261 (1988)
20. Dickmanns, E.D., Mysliwetz, B.D.: Recursive 3-d road and relative ego-state estimation. *IEEE Trans. Pattern Anal. Mach. Intell.* **14**, 199–213 (1992)
21. Raviv, D., Herman, M.: A nonreconstruction approach for road following. *Proc. SPIE Intell. Robots Comput. Vis.* **1608**, 2–12 (1992)
22. Sasiadek, J.Z., Dulba, I.: 3D local trajectory planner for UAV. *J. Intell. Robot. Syst* **29**, 191–210 (2000)
23. Sasiadek, J.Z., Dulba, I.: A heuristic approach to robot path planning based on task requirements using a genetic algorithm. *J. Intell. Robot. Syst* **16**, 65–88 (1996)
24. Cagigas, D., Abascal, J.: A hierarchical extension of the D* algorithm. *J. Intell. Robot. Syst* **42**, 393–413 (2005)
25. Wooden, D., Egerstedt, M.: On finding globally optimal paths through weighted colored graphs. In: Proc. of 45th IEEE Conf. on Decision and Control, pp. 3849–3854, San Diego, 13–15 December 2006

26. Sun, J., Mehta, T., Wooden, D., Powers, M., Regh, J., Balch, T., Egerstedt, M.: Learning from examples in unstructured, outdoor environments. *J. Field Robot.* **23**, 1019–1036 (2006)
27. Wooden, D., Egerstedt, M.: Oriented visibility graphs: Low-complexity planning in real-time environments. In: *Proc. of IEEE Conf. on Robotics and Automation*, pp. 2354 – 2359, Orlando, May 2006
28. Wooden, D.: A guide to vision-based map building. *IEEE Robot. Autom. Mag* **13**, 94–98 (2006)
29. Hespanha, J.P., Morse, A.S.: Stability of switched systems with average dwell-time. In: *Proc. of 38th IEEE Conference on Decision and Control*, pp. 2655–2660, Phoenix, 7–10 December 1999
30. Liberzon, D., Morse, A.S.: Benchmark problems in stability and design of switched systems. *IEEE Control Syst. Mag.* **19**, 59–70 (1999)
31. Branicky, M.: Multiple lyapunov functions and other analysis tools for switched and hybrid systems. *IEEE Trans. Automat. Contr.* **43**(4), 475–482 (1998)
32. DeCarlo, S.P.R., Branicky, M.S., Lennartson, B.: Perspectives and results on the stability and stabilizability of hybrid systems. *Proc. IEEE* **88**(2), 1069–1082 (2000)
33. Tomlin, C., Sastry, S.: Switching through singularities. In: *Proc. of 36th IEEE Conf. on Decision and Control*, pp. 1–6, San Diego, 10–12 December 1997
34. Khalil, H.K.: *Nonlinear Systems*, 3rd ed. Prentice Hall, Englewood Cliffs (2002)
35. Calabi, E., Olver, P.J., Shakiban, C., Tannenbaum, A., Haker, S.: Differential and numerically invariant signature curves applied to object recognition. *Int. J. Comput. Vis.* **26**, 107–135 (1998)
36. Zhang, F., Leonard, N.: Generating contour plots using multiple sensor platforms. In: *Proc. of IEEE Symposium on Swarm Intelligence*, pp. 309–314, Pasadena, 8–10 June 2005
37. Duttagupta, S., Ramamritham, K., Ramanathan, P.: Distributed boundary estimation using sensor networks. In: *Proc. of IEEE International Conference on Mobile Adhoc and Sensor Systems (MASS)*, pp. 316–325, Vancouver, 9–12 October 2006